SERCA function is impaired in skeletal and cardiac muscles from young DBA/2J mdx mice

Riley EG Cleverdon[1,2], Kennedy C Whitley[1,2], Daniel M Marko[3], Sophie I Hamstra[1,2], Jessica L Braun[1,2], Brian D Roy[1,2], Rebecca EK MacPherson[3,4], Val A Fajardo[1,2,4]*

[1] Department of Kinesiology, Brock University, St. Catharines, Ontario, Canada.
[2] Centre for Bone and Muscle Health, Brock University, St. Catharines, Ontario, Canada.
[3] Department of Health Sciences, Brock University, St. Catharines, ON L2S 3A1, Canada.
[4] Centre for Neuroscience, Brock University, St. Catharines, ON L2S 3A1, Canada.

Corresponding author:
Val A. Fajardo, PhD
Assistant Professor
Department of Kinesiology
Brock University
1812 Sir Isaac Brock Way
L2S 3A1
vfajardo@brocku.ca

Summary (150 word max)

The DBA/2J (D2) *mdx* mouse has emerged as a more severe model of Duchenne muscular dystrophy when compared to the traditional C57BL/10 (C57) *mdx* mouse. Here, we questioned whether sarco(endo)plasmic reticulum Ca^{2+}-ATPase (SERCA) function would differ in muscles from young D2 and C57 *mdx* mice. In gastrocnemius muscles, both D2- and C57 *mdx* mice exhibited signs of impaired Ca^{2+} uptake, however, this was more severe in D2 *mdx* mice. Maximal SERCA activity was lowered only in D2 *mdx* gastrocnemius muscles and not C57 *mdx* muscles. Furthermore, in the left ventricle and diaphragm, Ca^{2+} uptake was impaired in C57 *mdx* muscles with lowered rates of Ca^{2+} uptake compared with C57 WT mice, whereas in muscles from D2 *mdx* mice, rates of Ca^{2+} uptake were unattainable due to the severe impairments in their ability to transport Ca^{2+}. Overall, our study demonstrates that SERCA function is drastically impaired in young D2 *mdx* mice.

Keywords: SERCA, sarcolipin, muscular dystrophy, energy expenditure, RYR, calcium leak, reactive oxygen species, reactive nitrogen species

46 **INTRODUCTION**

47 Duchenne muscular dystrophy (DMD) is an X-linked recessive muscle wasting disease,
48 affecting approximately 1 in 5,000 boys worldwide (Mah et al., 2014; Mendell et al., 2012).
49 Symptoms of DMD typically begin at three or four years of age and with no cure to date, patients
50 usually succumb to cardiorespiratory complications from the disease by the third or fourth decade
51 of life (Emery, 2002; Mavrogeni et al., 2015; Straub et al., 2016). Caused by the complete loss of
52 dystrophin, a protein that normally connects the cytoskeleton and extracellular matrix to the
53 sarcolemma, DMD is characterized by excessive membrane tearing and myofibre
54 damage/degeneration (Blake et al., 2002). Loss of dystrophin is the initial insult of DMD, however
55 there are several secondary consequences of the disease including chronic inflammation, oxidative
56 stress, and calcium (Ca^{2+}) overload (Tubridy et al., 2001). Combined, these processes ultimately
57 lead to the pathological hallmarks of DMD which include degeneration, necrosis, and fatty and
58 fibrotic replacement of muscular tissue (Shin et al., 2013).

59 Ca^{2+} is a potent signaling molecule largely responsible for excitation-contraction coupling
60 (ECC) in skeletal and cardiac muscle. Two major Ca^{2+} regulatory proteins involved in muscle ECC
61 are the ryanodine receptor (RyR) and sarco-endoplasmic reticulum ATPase (SERCA) pump,
62 located in the sarcoplasmic reticulum (SR). RyR is responsible for the release of Ca^{2+} from the SR
63 into the myoplasm, which initiates cross-bridge formation and force generation, whereas SERCA
64 catalyzes the reuptake of Ca^{2+} into the SR to initiate muscle relaxation (Santulli et al., 2018;
65 Tupling, 2004; Tupling, 2009). However, several studies have shown that if SR Ca^{2+} handling is
66 dysregulated, Ca^{2+} can become chronically elevated in the myoplasm, leading to muscle damage
67 and weakness. Indeed, impaired Ca^{2+} handling is a major part of the pathology in the muscles of
68 patients living with DMD. The resulting Ca^{2+} overload exacerbates oxidative stress, inflammation,

69 and cellular necrosis which in turn perpetuates dystrophic pathology (Robert et al., 2001; Turner
70 et al., 1988). SERCA specifically has been implicated in dystrophic muscles, and several studies
71 have shown that SERCA is impaired in skeletal and cardiac muscles from the murine
72 C57BL/10ScSn (C57) *mdx* model of DMD (Gehrig et al., 2012; Schneider et al., 2013; Voit et al.,
73 2017). This is in part due to elevations in reactive oxygen and nitrogen species (RONS) in *mdx*
74 muscle that can damage the SERCA pumps (Gehrig *et al.*, 2012). The SERCA pumps contain
75 several residues that are susceptible to RONS mediated modifications such as nitrosylation and
76 nitration, ultimately impairing their ability to transport Ca^{2+} (Viner et al., 1996; Viner et al., 1999a;
77 Viner et al., 1997; Viner et al., 1999b).

78 The C57 *mdx* mouse, originally discovered in 1984 (Bulfield et al., 1984), has served as
79 the dominant *in vivo* model to study cellular mechanisms and potential therapies for DMD.
80 However, with a mild dystrophic pathology that is slow to progress, researchers have sought out
81 alternative models that may better recapitulate human DMD (Swiderski and Lynch, 2021). For
82 example, previous research has shown that SERCA pump function is more severely impaired in
83 the *mdx*/utrophin double knockout (dko) mouse (Schneider *et al.*, 2013; Voit *et al.*, 2017) – a
84 severe DMD mouse model where both dystrophin and its functional homolog utrophin are
85 completely absent (Deconinck et al., 1997; Grady et al., 1997). This suggests that SERCA
86 dysfunction progresses along with disease severity, whereby more severe models of DMD will
87 display more severe impairments in SERCA function.

88 More recently, the traditional C57 *mdx* mouse was backcrossed onto a DBA/2J
89 background, giving way to the D2.B10-Dmd^{mdx}/J (D2 *mdx*) mouse (Coley et al., 2016). Unlike the
90 C57 *mdx* mouse, the D2 *mdx* mouse presents with a juvenile onset and more severe DMD
91 pathology, including pronounced muscle weakness and damage, degeneration, fibrosis, necrosis,

92 and inflammation (Coley *et al.*, 2016; Hammers et al., 2020; van Putten et al., 2019). The
93 underlying mechanisms behind the greater pathology displayed in D2 *mdx* mice compared to C57
94 *mdx* mice are still under investigation, though a recent report has implicated elevated TGF- β
95 signalling (Mázala et al., 2020). However, to our knowledge SERCA function has yet to be
96 characterized in the D2 *mdx* mouse. Therefore, we examined SERCA function in 8-10-week-old
97 D2 and C57 *mdx* mice. This cohort was selected based on previous studies showing that D2 *mdx*
98 mice at this age display muscle weakness and pathology whereas the C57 *mdx* mice do not (Coley
99 *et al.*, 2016; Hammers *et al.*, 2020; van Putten *et al.*, 2019). We hypothesized that severity in
100 pathology related to weakness observed in D2 *mdx* mice compared to the C57 *mdx* mice would be
101 associated with greater impairments to SERCA function.
102
103 **RESULTS**
104 ***Muscle weakness and wasting in the C57 mdx versus D2 mdx mice***
105 We first sought to verify the phenotypical weakness and atrophy previously reported in the
106 D2 *mdx* mice. As expected, serum CK was elevated in both C57 and D2 *mdx* mice, denoted with
107 a significant main effect of *mdx* genotype (Figure 1A). Moreover, gastrocnemius muscle and body
108 mass were significantly lower in the D2 strain, indicating that mice on the D2 background are
109 generally smaller. Interestingly, a significant interaction between background strain and *mdx*
110 genotype showed that body mass was lower in D2 *mdx* vs D2 WT mice (Figure 1B and C). In
111 contrast, there were no differences in body mass with C57 *mdx* and C57 WT mice. When
112 normalized to body mass, a significant main effect of background strain was found suggesting that
113 the gastrocnemius:body mass ratio was lower in mice on the D2 background compareed with those
114 on a C57 background (Figure 1D). However, there were no differences in comparisons between

115 WT and *mdx* mice for either C57 or D2 strains. Holding impulse, or hangwire time normalized to
116 body mass, was significantly lower across both C57 *mdx* and D2 *mdx* mice compared with their
117 respective WT groups as denoted by a significant main effect of *mdx* genotype (Figure 1E).
118
119 ***Metabolic phenotyping of the C57 mdx and D2 mdx mice***
120 Mice were housed in the Promethion metabolic cage system (48 hour periods) to examine
121 cage activity, energy expenditure and various behavioural characteristics. Our data shows that D2
122 *mdx* mice were less ambulant in their cages compared with D2 WT mice with a main effect of *mdx*
123 genotype measued across the light, dark and total daily phases (Figure 2A). However, we did not
124 observe any differences in cage activity in C57 *mdx* mice compared with C57 WT mice, which is
125 consistent with earlier-onset muscle weakness and wasting previously found in D2 *mdx* mice
126 (Coley *et al.*, 2016; Hammers *et al.*, 2020; van Putten *et al.*, 2019). Along with cage activity, we
127 found that D2 *mdx* mice, but not C57 *mdx* mice had significantly elevated energy expenditure
128 when compared to their respective WT groups (Figure 2 C and D). This was denoted as a
129 significant main effect of *mdx* genotype in D2 mice (Figure 2C). Interestingly, this increase in
130 daily energy expenditure in D2 *mdx* mice was met with a significant reduction in daily food intake
131 compared with D2 WT mice (Figure 2E). We did not observe such changes in C57 *mdx* vs C57
132 WT mice (F). We also did not observe any changes in water intake across any experimental groups
133 (Figure 2G and H). The Promethion metabolic cage system also allows for certain behavioural
134 analyses including time spent in or touching its 'home' – a habitat enclosure on a slightly elevated
135 platform. Our results show that D2 *mdx* mice spent less time in the home compared with D2 WT
136 mice, however, this did not reach statistical significance (Figure 2I). There were no differences
137 detected between C57 *mdx* and C57 WT mice (Figure 2J). We did find that D2 *mdx* mice spent

138 significantly less time interacting or touching the habitat compared with D2 WT mice (Figure 2K),
139 however, this was not observed in C57 *mdx* and C57 WT mice (Figure 2L). As the home is in an
140 elevated platform, we believe that this serves as an additional indication of muscle weakness,
141 whereby the D2-*mdx* mice were not strong enough to enter the elevated enclosure.
142
143 ***Ca^{2+} uptake and SERCA activity is impaired in D2 mdx mice but not C57 mdx mice***
144 We then examined SERCA function in gastrocnemius muscles from C57 and D2 -WT and
145 -*mdx* mice (Figure 3). Ca^{2+} uptake experiments revealed obvious impairments in both C57 and D2
146 *mdx* mice (Figure 3A). Traditionally, rates of Ca^{2+} uptake would be examined using tangent
147 analysis at a free Ca^{2+} concentration of 1000-2000 nM (Fajardo et al., 2015). However, for both
148 C57 *mdx* and D2 *mdx* mice we could not utilize such approach as the Ca^{2+} uptake curve failed to
149 cross 2000 and 1000 nM, which is indicative of impaired SERCA function. Alternatively, we
150 examine the area-under-the-curve (AUC) and total Ca^{2+} taken in during the 400 s protocol (Figure
151 3B and C). For both, we found a significant main effect of *mdx* genotype with elevated AUC and
152 lowered total Ca^{2+} uptake, suggesting that both C57 and D2 *mdx* mice have impaired SERCA
153 function. However, we also note a significant interaction with background strain and *mdx*
154 genotype, that shows that the elevation in AUC and reduction in total Ca^{2+} uptake is far more
155 prominent in D2 *mdx* muscles (Figure 3B and C).
156 To further explore the impairments in SERCA function, we then measured Ca^{2+}-dependent
157 SERCA activity in the gastrocnemius muscle (Figure 3D and E). SERCA activity-*p*Ca curves show
158 a selective impairment in D2 *mdx* gastrocnemius muscles; however, two-way ANOVA analysis
159 did not reveal a significant interaction ($p = 0.06$, Figure 3F). No changes in SERCA's apparent
160 affinity for Ca^{2+} (pCa_{50}) were found (Figure 3G). Nonetheleless, our findings show that SERCA

161 function is impaired in C57 and D2 *mdx* muscle, however, it the level of impairment is more
162 prominent in the D2 *mdx* gastrocnemius muscle. To determine a potential pathological
163 consequence of Ca^{2+} dysregulation calpain activity was measured in the gastrocnemius. We found
164 that calpain activity was significantly higher in the C57 and D2 *mdx* muscles compared with C57
165 and D2 WT, as denoted by a significant main effect of *mdx* genotype (Figure 3H). In addition, a
166 significant main effect of background strain indicates that D2 mice (WT and *mdx*) had greater
167 calpain activity compared to C57 mice (Figure 3K). Furthermore, planned comparisons between
168 D2 *mdx* and C57 *mdx* showed that calpain activity was significantly higher in D2 *mdx* mice (p =
169 0.0006, Student's t-test).
170
171 ***Elevated RONS may contribute to impaired SERCA function***
172 To examine the potential mechanisms explaining the drastic imapirments in SERCA
173 function found in D2 *mdx* muscles, we performed western blotting of SR Ca^{2+} handling proteins
174 (Figure 4). Our results showed that SERCA1 content was upregulated in both C57 and D2 *mdx*
175 mice with a significant main effect of *mdx* genotype (Figure 4A and B). A similar main effect was
176 found with SERCA2 content, however, a significant interaction between *mdx* genotype and
177 background strain indicated that the increase in SERCA2 was most prominent in D2 *mdx* muscle
178 (Figure 4A and C). Sarcolipin (SLN) is a known inhibitor of SERCA that is upregulated in *mdx*
179 mice (Fajardo et al., 2018; Schneider *et al.*, 2013) and was ectopically expressed in both the D2
180 *mdx* and C57 *mdx* gastrocnemius muscle. That is, WT gastrocnemius muscles from WT C57 and
181 D2 *mice* do not typically express SLN protein, and SLN could only be detected via western blot
182 only in the *mdx* mice (Supplementary Figure 1). Interestingly, SLN content in D2 *mdx*
183 gastrocnemius muscles was significantly lower compared with C57 *mdx* gastrocnemius muscle

184 (Figure 4D). We then examined RyR1 content, and found that in both C57 and D2 *mdx* muscles,
185 RyR1 was lower compared with C57 and D2 WT, with a significant main effect of *mdx* genotype
186 (Figure 4E).RyR1 content in D2 mice (both WT and *mdx*) appeared to be lower than that found in
187 C57 mice, but this was not statistically significant (Figure 4E). Calstabin, the channel stabilizer
188 of RyR1 did not have any significant changes in protein content (Figure 4F). We also investigated
189 protein nitrosylation and nitration in the gastrocnemius under reducing conditions to determine
190 levels of irreversible RONS modification, since elevated RONS can impair SERCA function
191 (Viner *et al.*, 1996; Viner *et al.*, 1999a; Viner *et al.*, 1997; Viner *et al.*, 1999b). Our results show
192 that *mdx* mice (both C57 and D2) have elevated RONS levels compared with WT, with a main
193 effect of *mdx* genotype. Furthermore, a significant interaction between *mdx* genotype and
194 background strain shows that the elevations in total nitrocysteine and and nitrotyrosine were most
195 prominent in D2 *mdx* mice (Figure 4G and H).
196
197 ***Ca^{2+} uptake is also impaired in D2 mdx left ventricle and diaphragm muscles***
198 Given the cardiorespiratory implications of DMD, we also assessed SERCA function in
199 cardiac (left ventricle) and diaphragm muscles from C57 and D2 -WT and -*mdx* mice. Similar to
200 our results with the gastrocnemius, we found that D2 *mdx* mice had severe decrements in Ca^{2+}
201 uptake in both the cardiac and diaphragm muscles (Figure 5). In the cardiac muscle, Ca^{2+} uptake
202 curves show a drastic impairment in Ca^{2+} transport in D2 *mdx* mice, which translated to a
203 significant elevation in AUC when compared with D2 WT mice (Figure 5A and B). Though AUC
204 was not different between C57 *mdx* and C57 WT mice, we were able to measure Ca^{2+} uptake rates
205 at a free Ca^{2+} of 1000 nM. In doing so, we found a significant reduction in Ca^{2+} uptake rate in the
206 LV from C57 *mdx* mice compared with C57 WT mice (Figure 5C). Similar findings were found
207 in the diaphragm, where there were drastic impairments in Ca^{2+} uptake in the D2 *mdx* diaphragm

208 that led to a significantly higher AUC compared with D2 WT mice (Figure 5D and F). Moreover,
209 comparing Ca^{2+} uptake rates at 1000 nM, shows a significant difference between C57 WT and C57
210 *mdx* diaphragm muscles, with rates being lower in the latter (Figure 5F). Altogether, these results
211 show that while Ca^{2+} uptake is indeed impaired in C57 *mdx* muscles, the impairment appears to be
212 more prominent in D2 *mdx* muscles where rates of Ca^{2+} uptake were unattainable.
213
214 **DISCUSSION**
215 To our knowledge, this study is the first to compare SERCA function in both the D2 *mdx*
216 mouse and C57 *mdx* mouse model. The D2 *mdx* mouse is known as a more severe DMD model
217 with early onset weakness compared to the C57 *mdx* mouse. Impulse and measures of cage
218 ambulation supported this showing that D2 *mdx* mice had early onset muscle weakness occurring
219 at 8-10 weeks of age. Also, the D2 *mdx* mice had less interaction with the elevated mouse home
220 enclosure compared to C57 *mdx* mice, suggesting that these mice were less able to jump onto this
221 raised platform found within their cages. Interestingly, D2 *mdx* mice also had a hypermetabolic
222 profile, where these mice had the highest levels of energy expenditure while ambulating the least,
223 which we believe can contribute to the smaller body and muscle mass commonly observed in these
224 mice. Perhaps inconsistent with our results, a previous study found that energy expenditure was
225 elevated in 5 month old C57 *mdx* mice compared with WT mice (Strakova et al., 2018). We believe
226 that this discrepancy could possibly be explained by age differences, as our C57 *mdx* mice were
227 younger as compared to the mice used in the study by Strakova and colleagues.
228 To explain why the D2 *mdx* mice are much weaker at an earlier age, we explored the
229 involvement of SERCA dysfunction. Our Ca^{2+} uptake results showed that D2 *mdx* muscles
230 (gastrocnemius, cardiac and diaphragm) had obvious impairments in their ability to bring Ca^{2+} into
231 the SR. This manifested as an elevated AUC during the uptake period. Importantly, several studies

232 have shown that C57 *mdx* muscles exhibit impairments in SERCA function (Gehrig *et al.*, 2012;
233 Schneider *et al.*, 2013; Voit *et al.*, 2017). The findings presented in this study are consistent with
234 this as C57 *mdx* gastrocnemius also had elevated AUC during the Ca^{2+} uptake protocol, and C57
235 *mdx* LV and diaphragm had significantly slower rates of Ca^{2+} uptake compared with C57 WT
236 counterparts. However, the fact that Ca^{2+} uptake was so dramatically impaired in D2 *mdx* mice
237 that rates of Ca^{2+} uptake at 1000-2000 nM free [Ca^{2+}] could not be attained, in combination with
238 lowered maximal SERCA activity, suggests that the impairment in SERCA function is most
239 prominent in D2 *mdx* muscles. Altogether, our finding is consistent with a previous study showing
240 that SERCA dysfunction proceeds on a continuum of disease severity, where more severe
241 dystrophic models such as the dko mouse (Schneider *et al.*, 2013) and the D2 *mdx* mouse have
242 more severe impairments in SERCA function.

243 The alterations to SERCA pump function do not seem to be explained by differences in
244 SERCA protein levels. Both SERCA1 and SERCA2 were upregulated in the gastrocnemius, which
245 we believe is an adaptive response aimed at improving SR Ca^{2+} handling. Indeed, SERCA density
246 is an important determinant of SR Ca^{2+} filling, at least in healthy conditions (Tupling, 2004).
247 However, any compensatory increase in SERCA content/density was unsuccessful in the rescuing
248 SERCA function. We next examined SLN expression. Although it is not typically expressed in
249 murine gastrocnemius muscle, ectopic expression of SLN occurred in both *mdx* mouse models,
250 with SLN protein being elevated to a greater extent in the C57 *mdx* mice compared to the D2 *mdx*
251 mice. Studies have shown that SLN is upregulated along with disease progression with its
252 expression being further upregulated in the dko mice compared with *mdx* mice (Schneider *et al.*,
253 2013). Furthermore, knocking out SLN in mdx and dko mice improved dystrophic pathology
254 suggesting that SLN may contribute to *mdx* pathology by improving SERCA function

255 (Balakrishnan et al., 2022; Mareedu et al., 2021; Voit *et al.*, 2017). However, there are discrepant
256 results with SLN deletion studies also impairing *mdx* pathology (Fajardo *et al.*, 2018) or not
257 improving phenotype (data not shown in ref (Bal et al., 2021)). The reasons for these discrepant
258 results are unclear, however, a point on hormesis was recently raised (Chambers et al., 2022).
259 Since we found that SLN was less upregulated in the more severe D2 *mdx* mouse model with
260 dramatic impairments in SERCA function, our results could suggest that SLN may not be a critical
261 player in the SERCA function impairments and potentially *mdx* pathology in the D2 *mdx* mouse;
262 however, this should be investigated further specifically in the D2 *mdx* mouse.

263 In addition, SLN is a known uncoupler of SERCA that uncouples Ca^{2+} transport from ATP
264 hydrolysis (Bombardier et al., 2013; Smith et al., 2002). Thus, its upregulation in the D2 *mdx*
265 mouse may contribute to the observed increase in daily energy expenditure. However, since we
266 found that SLN levels were relatively higher in the C57 *mdx* vs D2 *mdx* mice, other potential
267 mechanisms may be contributing to the increased daily energy expenditure found specifically in
268 D2 *mdx* mice. One potential factor may be elevated oxidative/nitrosative stress as SERCA is
269 susceptible to damaging RONS modifications such as nitrosylation and nitration (Viner *et al.*,
270 1996; Viner *et al.*, 1999a; Viner *et al.*, 1997; Viner *et al.*, 1999b). Consistent with our observations
271 of a prominent elevation in total nitrocysteine and nitrotyrosine levels in D2 *mdx* muscles, it is
272 plausible that RONS modifications could be contributing to the changes in SERCA function. That
273 is, our results of elevated total protein nitrosylation and tyrosine nitration under reducing
274 conditions are suggestive of irreversible RONS modifications that may be impairing the SERCA
275 pump. Moreover, damage to the SR membrane itself from RONS may contribute to the drastic
276 impairments in Ca^{2+} uptake found in D2 *mdx* muscles. While we note that maximal SERCA
277 activity appeared to be lower in the D2 *mdx* mouse, there still was an appreciable amount of

278 SERCA-mediated ATP hydrolysis. Combined with an obvious inability to bring Ca^{2+} into the SR,
279 our results could suggest that the SERCA pumps have become highly inefficient in D2 *mdx* muscle
280 – hydrolyzing ATP while bringing only minimal levels of Ca^{2+} into the SR. This uncoupling effect
281 could potentially contribute to the elevated daily energy expenditure found in the D2 *mdx* mice.

282 We also determined the activation of calpain in D2 *mdx* gastrocnemius muscles. Calpain
283 is a Ca^{2+}-dependent proteolytic enzyme previously shown to be more active in *mdx* muscles (Gailly
284 et al., 2007). To our knowledge, ours is the first study to demonstrate that rates of calpain activity
285 are higher in the D2 background strain compared to C57, irrespective of the *mdx* genotype.
286 Furthermore, planned comparisons between D2 *mdx* and C57 *mdx* mice specifically revealed a
287 significant 2.2-fold increase in calpain activity in the former vs the latter ($p = 0.0006$ via Student's
288 t-test). This finding is important and adds mechanistic insight that may partly explain the worsened
289 pathology in the D2 *mdx* mouse. It is interesting that the D2 WT mice already had elevated calpain
290 activation compared with C57 WT. This apparent difference in background strain may provide
291 additional insight as to why *mdx* mice on the D2 background are worse off than *mdx* mice on the
292 C57 background. One explanation that is not yet well understood, is a potential crosstalk between
293 calpain activation and the pro-fibrotic factor TGF-β. Previous studies have found that TGF-β1
294 upregulation in lung fibroblasts (Li et al., 2015) and atrial derived myocytes (Yeh et al., 2011) can
295 increase calpain activation . This is interesting given recent findings showing that a polymorphism
296 of LTBP4 in D2 WT mice greatly upregulates TGF-β (Heydemann et al., 2009; Mázala *et al.*,
297 2020), suggesting that the increased TGF-β activity could increase calpain activity in the D2 WT
298 mice. This combined with the impairments observed in SERCA function could contribute to
299 elevated calpain in the D2 *mdx* mice.

300 In conclusion, our study clearly shows drastic impairments in SERCA function in skeletal
301 and cardiac muscles from D2 *mdx* mice. Our results suggest that the early onset weakness and
302 damage observed in young D2 *mdx* mice may be partly due to an inability to bring Ca^{2+} into the
303 SR. Future studies should investigate whether improving SERCA function, potentially through
304 cytotoxic protection against RONS may mitigate dystrophic pathology and improve physiological
305 outcomes in the D2 *mdx* mouse.
306
307 **LIMITATIONS TO THE STUDY**
308 Our study clearly shows that SERCA function is severely impaired early on in D2 *mdx*
309 mice and may contribute to the severity of muscle weakness and damage. However, we
310 acknowledge that our work is largely descriptive, and future studies aimed at improving SERCA
311 function will determine its causal role, if any. Furthermore, the mechanisms leading to these
312 impairments in SERCA function are still unknown, and though we associate them with elevated
313 oxidative/nitrosative stress, SERCA-specific modifications should be assessed in the future. RyR
314 Ca^{2+} leak is another major player in the Ca^{2+} disturbances found in C57 *mdx* muscle (Bellinger et
315 al., 2009; Capogrosso et al., 2018). Our study is limited in that we did not examine RyR function.
316 Finally, our study does not discern whether the elevated daily energy expenditure in D2 *mdx* mice
317 is caused solely by increased muscle-based energy consumption. Other thermogenic organs such
318 as brown and beige fat could be investigated in the future.
319
320
321
322

ACKNOWLEDGEMENTS

This work was supported by an unrestricted Brock University internal grant and a Canada Research Chair Tier 2 in Tissue Plasticity and Remodelling to VAF. REGC and SIH were supported by a NSERC CGS-M, and JLB was supported by a CIHR CGS-M.

AUTHOR CONTRIBUTIONS

Riley EG Cleverdon: Conceptualization, methodology, validation, formal analysis, investigation, writing – original draft, visualization

Kennedy C Whitley: Methodology, investigation, formal analysis, writing – review & editing

Daniel M Marko: Methodology, investigation, formal analysis, writing – review & editing

Sophie I Hamstra: Investigation, formal analysis, writing – review & editing

Jessica L Braun: Investigation, formal analysis, writing – review & editing

Brian D Roy: Resources, writing – review & editing

Rebecca EK MacPherson: Resources, supervision, writing – review & editing

Val A Fajardo: Conceptualization, supervision, project administration, funding acquisition, investigation, formal analysis, visualization, writing – original draft

DECLARATION OF INTERESTS

The authors declare no competing interests.

352 **FIGURE LEGENDS**
353
354 **Figure 1: Creatine kinase, muscle/body mass and impulse:** A) Serum creatine kinase activity expressed
355 in units per litre. B) Gastrocnemius mass (mg), C) body mass (g), and D) gastrocnemius mass:body mass
356 ratio (mg:g). E) Impulse expressed as hangwire time*body mass. A two-way ANOVA was used for all
357 comparisons, n=12 per group (except for B and D, n = 6 per group). Values are represented as mean ± SEM.
358 Main effects and interactions expressed in bars over the graph, ****$p < 0.0001$ using a Sidak's post-hoc
359 test.
360
361 **Figure 2. Cage activity, energy expenditure and cage behaviour:** A) Daily cage ambulation in D2 mice
362 and B) C57 mice expressed in metres travelled. C) Energy expenditure in D2 mice and D) C57 mice
363 expressed in kcal/kg of body mass/hr. E) and G) Food (g) and water (mL) intake of D2 mice and F) and H)
364 C57 mice. Percentage of time spent in (I-Home) and interacting with (T-Home) the mouse home for D2
365 mice I) and K) and C57 mice J) and L). All metabolic cage analyses were measured over a 48-hour period.
366 Two-way repeated ANOVA examining the effect of time period, *mdx* genotype and their potential
367 interaction (A-H). **$p < 0.01$, *** $p < 0.001$, and ****$p < 0.0001$ using a Sidak's post-hoc test, n = 5-6 per
368 group. Student's t-test examined WT versus mdx (I-L), n = 5-6 per group. Values are represented as mean
369 ± SEM.
370
371 **Figure 3: SR Ca^{2+} uptake/leak, SERCA and calpain activity in C57 and D2 -WT and -*mdx***
372 **gastrocnemius muscle:** A) Ca^{2+} uptake curves from gastrocnemius homogenates. B) Area under the curve
373 (AUC) of Ca^{2+} uptake curves. C) Total Ca^{2+} uptake normalized to wet tissue weight. D & E) Ca^{2+}-dependent
374 SERCA activity curves in D2 and C57 -WT and -*mdx* gastrocnemius muscles. F) Maximal SERCA activity
375 expressed as μmol/g of protein/min and G) pCa_{50} of SERCA activity, n = 4. H) Calpain activity in
376 gastrocnemius muscles from D2 and C57 -WT and -*mdx* gastrocnemius muscles expressed as RFU min/mg
377 of protein. Two-way ANOVAs were performed with a Sidak's post-hoc test, *$p < 0.05$, **$p < 0.01$, ***p
378 < 0.001, and ****$p < 0.0001$ n= 5-6. Main effects and interactions expressed in bars over the graph. Values
379 are represented as mean ± SEM.
380
381 **Figure 4: Western blot analyses of SR Ca^{2+} handling proteins total protein nitrosylation and tyrosine**
382 **nitration:** A) Representative Western blot images for SERCA1 and SERCA2 and their respective semi-
383 quantificational analyses in gastrocnemius muscles from D2 and C57 -WT and *mdx* mice (B and C). D)
384 SLN content in gastrocnemius muscles from C57 *mdx* and D2 *mdx* muscles. E) RyR1 and F) calstabin
385 content in gastrocnemius muscles from D2 and C57 -WT and -*mdx.* G) Protein nitrosylation measured via
386 western blotting for nitrocysteine-adducted protein. H) Protein tyrosine nitration measured via western
387 blotting for nitrotyrosine-adducted protein. For B,C and E-H, a two-way ANOVAs were performed with a
388 Sidak's post-hoc test, **$p < 0.01$, ***$p < 0.001$, ****$p < 0.0001$ n = 6 per group. Main effects and
389 interactions expressed in bars over the graph. For D a Student's t-test was used, *$p < 0.05$, n = 6 per group.
390 All protein contents are expressed as arbitrary units. Values are represented as mean ± SEM.
391
392 **Figure 5: Ca^{2+} uptake in the cardiac and diaphragm muscles:** A) Ca^{2+} uptake curves from left ventricle
393 homogenates. B) AUC analysis in left ventricle homogenates. C) Ca^{2+} uptake rate in LV measured via
394 tangent analysis at 1000 nM free [Ca^{2+}]. D) Ca^{2+} uptake curves from diaphragm homogenates. E) AUC
395 analysis in diaphragm homogenates. F) Ca^{2+} uptake rate in diaphragm muscles measured via tangent
396 analysis at 1000 nM free [Ca^{2+}]. For B and E, Two-way ANOVAs were performed with a Sidak's post-
397 hoc test, ****$p < 0.0001$. For C and F, a Student's t-test was used, *$p < 0.05$. Main effects and interactions
398 expressed in bars over the graph. Values are represented as mean ± SEM, n = 5-6 per group.
399

STAR Methods

RESOURCE AVAILABILITY

Lead contact

Further information and requests for resources and reagents should be directed to and will be fulfilled by the lead contact, Val A. Fajardo (vfajardo@brocku.ca).

Materials availability

This study did not generate new unique reagents.

Data and code availability

All data are included in the published article or are available from the lead contact upon reasonable request. This paper does not report original code.

EXPERIMENTAL MODELS AND SUBJECT DETAILS

Mice and Design

Male C57 *mdx* (n = 12), C57 WT (n = 12), D2 *mdx* (n = 12), and D2 WT (n = 12) mice were purchased from Jackson Laboratories at 7-8 weeks of age. They were acclimated and housed in Brock University's Animal Facility, in an environmentally controlled room with a standard 12:12 hour light-dark cycle and allowed access to food and water *ad libitum*. After the mice reached 9-10 weeks of age, they were euthanized via cervical dislocation under general anesthetic (vaporized isoflurane) and their tissues were collected.

423 **METHOD DETAILS**

424 ***Hang Wire Testing***

425 At 8-9 weeks of age, mice were subjected to a hang wire test to determine limb strength
426 and endurance. All mice were gently placed on the wire situated 12 inches high and were left
427 suspended on the wire until they reached exhaustion and dropped from the wire to the base of the
428 cage. The time they remained suspended was recorded for three trials, separated by a 60s recovery
429 period. Impulse (s*g) was calculated according to DMD_M.2.1.004 standard operating procedures
430 by multiplying the average time suspended by body mass.

431

432 ***Metabolic Caging***

433 At 8-9 weeks of age, mice were housed in pairs in a Promethion Metabolic Cage System
434 for 48 hours. Two 12-hour light and dark cycles were measured, and data was collected. Food and
435 water intake were measured through mass changes with the MM-1 load cell, the Promethion mass
436 measurement device. Cage ambulation was quantified through metres travelled which is collected
437 through beam breaks with the BXYZ Beambreak Activity Monitor in the x y, and z planes.
438 Respiratory exchange ratio (RER) was calculated as VCO_2 (volume of carbon dioxide expired each
439 minute) divided by VO_2 (volume of oxygen inspired each minute) measured from the Promethion
440 metabolic cages equipped with O_2 and CO_2 gas analyzers. To obtain mean energy expenditure
441 expressed in kcal/hr, the Weir equation was used (41).

442

443 ***Sample Collection and Homogenization***

444 Gastrocnemius, diaphragm, and cardiac muscles (n=12/group) were rapidly extracted from
445 euthanized animals and flash frozen in liquid N2 and stored at -80˚C. For Ca^{2+} uptake and SERCA

446 activity analyses, muscles were homogenized in homogenizing buffer (5 mM HEPES, 250 mM
447 sucrose, 0.2 mM PMSF, 0.2% NaN3; pH 7.5). An aliquot of the muscle homogenate was then
448 supplemented with protease and phosphatase (phosSTOP; cOmplete Mini) inhibitors for western
449 blot analyses. Blood was collected via cardiac puncture and spun at 5000 x g for 8 minutes (4°C)
450 and serum was collected and stored at -80˚C.
451
452 ***Serum Creatine Kinase Activity***
453 Serum creatine kinase activity was determined as previously described (42), with a M2
454 Molecular Device plate reader and a commercially available assay (Cat. #C7522, Pointe Scientific
455 Inc., Canton, MI, USA) fitted onto a 96-well plate and calibrated with a standard curve of purified
456 creatine kinase (Sigma, Oakville, ON, Canada, Cat. 10127566001).
457
458 ***Ca^{2+} Uptake***
459 Ca^{2+} uptake assays were fitted onto a 96-well plate and done on a M2 Molecular Device
460 plate reader and the ratio-able Ca^{2+} fluorescent indicator Indo-1. In brief, 20 µl of diaphragm, 25
461 µl of gastrocnemius or 50 µl of left ventricle homogenate was added to 200 µl Ca^{2+} uptake buffer
462 (20mM HEPES, 200mM KCL, 10mM NaN_3, 5µM TPEN, 15mM $MgCl_2$, 5mM Oxalate; pH 7.0),
463 and 1 µl of Indo-1 (1 mM in 50 mM glycine, pH 7.0). Ca^{2+} uptake was initiated with 4 µl of ATP
464 (250 mM, pH 7.0) with the plate read kinetically set with an excitation wavelength of 355 nM and
465 emission wavelengths of 405 nm (Ca^{2+}-bound Indo-1) and 485 nm (Ca^{2+}-free Indo-1). Free Ca^{2+}
466 concentration was calculated using the following formula and a Kd of 250 nM for Indo-1. The
467 amount of Ca^{2+} uptake were measured through an area under the curve analysis (AUC). In addition,
468 rates of Ca^{2+} uptake were analyzed and normalized to wet tissue weight in mg.

469

470 $$[Ca^{2+}] = K_d \left(\frac{R - R_{min}}{R_{max} - R}\right)\left(\frac{S_{f2}}{S_{b2}}\right)$$

471

472 Formula 1: Free Calcium Concentration ($[Ca^{2+}]_f$)

473 K_d is the dissociation constant of Indo-1 (250 nM). R_{min} refers to the ratio of bound:unbound Indo-1 after
474 adding 15 mM EGTA. R_{max} refers to the ratio of bound:unbound Indo-1 after adding 5 M $CaCl_2$. S_{f2} is the
475 fluorescence emission at 485nm (Ca^{2+}-free Indo-1) in the EGTA portion and S_{b2} is the fluorescence
476 emission at 485nm in the 5 M $CaCl_2$ portion.

477

478 ***SERCA ATPase Activity***

479 Ionophore (A23187; Sigma Aldrich) supported SERCA activity was measured in
480 gastrocnemius homogenates using an enzyme-linked spectrophotometric assay as previously
481 described (24, 30, 43). Briefly, muscle homogenates (15 µl), pyruvate kinase (PK) and lactate
482 dehydrogenase (LDH) (18 U I^{-1} for both) were added to Ca^{2+} ATPase buffer (20mM HEPES,
483 200mM KCl, 10mM NaN3, 1mM EGTA, 15mM MgCl2, 5mM ATP, 10mM
484 phosphoenolpyruvate). To initiate SERCA activity, 4 µl of 1.9% (w/v) NADH was added and the
485 plates were then read at 340 nm for 30 minutes. SERCA-dependent activity in gastrocnemius
486 homogenates was calculated with a pathlength correction, extinction coefficient of NADH (6.22
487 mM), and the subtraction of ATPase activity in the presence of 1 µl SERCA-specific inhibitor,
488 CPA (40 mM) from total ATPase activity across a range of Ca^{2+} concentrations (*p*Ca 6.95 – 5.75).
489 A bicinchoninic acid (BCA) assay was done to normalize SERCA activity to grams of protein.

490

491 ***Western Blotting***

492 Western blotting was conducted to determine protein expression of SERCA1a/2a,
493 sarcolipin (SLN), RyR1 and calstabin. Laemmli buffer was added to muscle homogenates to
494 solubilize proteins that were then electrophorectially separated at 240V for 22 minutes on a 7-12%
495 TGX gradient gel (BioRad). Proteins were transferred to PVDF or nitrocellulose membranes for 6

496 minutes using BioRad Trans Blot Turbo. Prior to blocking, SuperSignal western Blot Enhancer
497 (46641) from Thermo Scientific was applied for the SLN blot. A 5% (w/v) milk and TBST solution
498 was used to block the membranes for one hour. Primary antibody was then added and incubated
499 overnight at 4°C. The primary antibodies SERCA1a (MA3-911), SERCA 2a (MA3-919), RYR1
500 (MA3-925) and calstabin (PA1-026A) were obtained from ThermoFisher Scientific (Waltham,
501 MA, USA). The primary antibody for SLN (ABT13) was obtained from Sigma-Aldrich (Oakville,
502 ON, CA). The primary antibody for nitrocysteine (ab94930) was obtained from Abcam
503 (Cambridge, UK). The primary antibody for nitrotyrosine (189542) was obtained from Cayman
504 Chemical (Ann Arbor, MI, USA). Subsequent to primary incubation, the membranes were washed
505 three times with TBST and then incubated with anti-mouse (SERCA1a/2a, RyR1 ;7076; Cell
506 Signalling Technology) or anti-rabbit (calstabin, SLN; 7074, Cell Signalling Technology,)
507 secondary antibodies at room temperature for 1 hour. The membranes were then washed again
508 three times with TBST then chemiluminescent substrate Millipore Immobilon (WBKLS0500;
509 Sigma-Aldrich) or SuperSignal West Femto Maximum Sensitivity Substrate (34095; Thermo
510 Scientific) was added prior to imaging with a BioRad Chemidoc. Optical densities were analyzed
511 with imageLab (BioRad) and normalized to total protein visualized with a ponceau stain (59803;
512 Cell Signalling Technology).
513
514 ***Calpain Activity Assay***
515 A commercialized calpain assay (QIA120; Millipore Sigma) was used in order to
516 determine calpain activity in the gastrocnemius. Tissue was freshly homogenized in RIPA lysis
517 buffer and 50 μl of sample was loaded in duplicate in either 100 μl of activator buffer or 100 μl of
518 inhibitor buffer in a 96-well plate as per the manufacturer's instructions. Then, 50 μl of diluted

519 substrate was added in the dark into each well and the plate was incubated for 15 minutes. The
520 plate was then measured for 10 minutes as a kinetic plate at an excitation of 370 nm and emission
521 of 450 nm to determine the rate of calpain activity normalized to total protein (via BCA assay).
522
523 ***Ethics statement***
524 All animal procedures were approved by the Brock University Animal Care and Utilization
525 Committee (file #17-06-03) and were carried out in accordance with the Canadian Council on
526 Animal Care guidelines.
527
528 **QUANTIFICATION AND STATISTICAL ANALYSIS**
529 ***Statistical analysis***
530 A two-way ANOVA was used to test the main effects of genotype (*mdx*) and strain (C57
531 or D2) and their potential interaction for most analyses. Post-hoc testing was completed using
532 Sidak multiple comparison testing. A Student's t-test was also used to compare cage ambulation
533 data. Statistical tests were conducted using GraphPad Prism 8 Software (San Diego, USA). All
534 values are presented as means ± standard error. Statistical significance is set to $p \leq 0.05$.
535
536
537
538
539

References

Bal, N.C., Gupta, S.C., Pant, M., Sopariwala, D.H., Gonzalez-Escobedo, G., Turner, J., Gunn, J.S., Pierson, C.R., Harper, S.Q., Rafael-Fortney, J.A., and Periasamy, M. (2021). Is Upregulation of Sarcolipin Beneficial or Detrimental to Muscle Function? Front Physiol *12*, 633058. 10.3389/fphys.2021.633058.

Balakrishnan, R., Mareedu, S., and Babu, G.J. (2022). Reducing sarcolipin expression improves muscle metabolism in mdx mice. Am J Physiol Cell Physiol *322*, C260-c274. 10.1152/ajpcell.00125.2021.

Bellinger, A.M., Reiken, S., Carlson, C., Mongillo, M., Liu, X., Rothman, L., Matecki, S., Lacampagne, A., and Marks, A.R. (2009). Hypernitrosylated ryanodine receptor calcium release channels are leaky in dystrophic muscle. Nat Med *15*, 325-330. 10.1038/nm.1916 nm.1916 [pii].

Blake, D.J., Weir, A., Newey, S.E., and Davies, K.E. (2002). Function and genetics of dystrophin and dystrophin-related proteins in muscle. Physiol Rev *82*, 291-329. 10.1152/physrev.00028.2001.

Bombardier, E., Smith, I.C., Vigna, C., Fajardo, V.A., and Tupling, A.R. (2013). Ablation of sarcolipin decreases the energy requirements for Ca2+ transport by sarco(endo)plasmic reticulum Ca2+-ATPases in resting skeletal muscle. FEBS Lett *587*, 1687-1692. 10.1016/j.febslet.2013.04.019 S0014-5793(13)00305-0 [pii].

Bulfield, G., Siller, W.G., Wight, P.A., and Moore, K.J. (1984). X chromosome-linked muscular dystrophy (mdx) in the mouse. Proc Natl Acad Sci U S A *81*, 1189-1192.

Capogrosso, R.F., Mantuano, P., Uaesoontrachoon, K., Cozzoli, A., Giustino, A., Dow, T., Srinivassane, S., Filipovic, M., Bell, C., Vandermeulen, J., et al. (2018). Ryanodine channel complex stabilizer compound S48168/ARM210 as a disease modifier in dystrophin-deficient mdx mice: proof-of-concept study and independent validation of efficacy. Faseb j *32*, 1025-1043. 10.1096/fj.201700182RRR.

Chambers, P.J., Juracic, E.S., Fajardo, V.A., and Tupling, A.R. (2022). Role of SERCA and sarcolipin in adaptive muscle remodeling. Am J Physiol Cell Physiol *322*, C382-c394. 10.1152/ajpcell.00198.2021.

Coley, W.D., Bogdanik, L., Vila, M.C., Yu, Q., Van Der Meulen, J.H., Rayavarapu, S., Novak, J.S., Nearing, M., Quinn, J.L., Saunders, A., et al. (2016). Effect of genetic background on the dystrophic phenotype in mdx mice. Hum Mol Genet *25*, 130-145. 10.1093/hmg/ddv460.

Deconinck, A.E., Rafael, J.A., Skinner, J.A., Brown, S.C., Potter, A.C., Metzinger, L., Watt, D.J., Dickson, J.G., Tinsley, J.M., and Davies, K.E. (1997). Utrophin-dystrophin-deficient mice as a model for Duchenne muscular dystrophy. Cell *90*, 717-727.

Emery, A.E. (2002). The muscular dystrophies. Lancet *359*, 687-695. 10.1016/s0140-6736(02)07815-7.

Fajardo, V.A., Bombardier, E., McMillan, E., Tran, K., Wadsworth, B.J., Gamu, D., Hopf, A., Vigna, C., Smith, I.C., Bellissimo, C., et al. (2015). Phospholamban overexpression in mice causes a centronuclear myopathy-like phenotype. Dis Model Mech *8*, 999-1009. 10.1242/dmm.020859.

Fajardo, V.A., Chambers, P.J., Juracic, E.S., Rietze, B.A., Gamu, D., Bellissimo, C., Kwon, F., Quadrilatero, J., and Russell Tupling, A. (2018). Sarcolipin deletion in mdx mice impairs calcineurin signalling and worsens dystrophic pathology. Hum Mol Genet. 10.1093/hmg/ddy302.

584 Gailly, P., De Backer, F., Van Schoor, M., and Gillis, J.M. (2007). In situ measurements of calpain
585 activity in isolated muscle fibres from normal and dystrophin-lacking mdx mice. J Physiol *582*,
586 1261-1275. 10.1113/jphysiol.2007.132191.
587 Gehrig, S.M., van der Poel, C., Sayer, T.A., Schertzer, J.D., Henstridge, D.C., Church, J.E., Lamon,
588 S., Russell, A.P., Davies, K.E., Febbraio, M.A., and Lynch, G.S. (2012). Hsp72 preserves muscle
589 function and slows progression of severe muscular dystrophy. Nature *484*, 394-398.
590 10.1038/nature10980
591 nature10980 [pii].
592 Grady, R.M., Teng, H., Nichol, M.C., Cunningham, J.C., Wilkinson, R.S., and Sanes, J.R. (1997).
593 Skeletal and cardiac myopathies in mice lacking utrophin and dystrophin: a model for Duchenne
594 muscular dystrophy. Cell *90*, 729-738.
595 Hammers, D.W., Hart, C.C., Matheny, M.K., Wright, L.A., Armellini, M., Barton, E.R., and Sweeney,
596 H.L. (2020). The D2.mdx mouse as a preclinical model of the skeletal muscle pathology associated
597 with Duchenne muscular dystrophy. Sci Rep *10*, 14070. 10.1038/s41598-020-70987-y.
598 Heydemann, A., Ceco, E., Lim, J.E., Hadhazy, M., Ryder, P., Moran, J.L., Beier, D.R., Palmer, A.A.,
599 and McNally, E.M. (2009). Latent TGF-beta-binding protein 4 modifies muscular dystrophy in
600 mice. J Clin Invest *119*, 3703-3712. 10.1172/jci39845.
601 Li, F.Z., Cai, P.C., Song, L.J., Zhou, L.L., Zhang, Q., Rao, S.S., Xia, Y., Xiang, F., Xin, J.B., Greer, P.A.,
602 et al. (2015). Crosstalk between calpain activation and TGF-β1 augments collagen-I synthesis in
603 pulmonary fibrosis. Biochim Biophys Acta *1852*, 1796-1804. 10.1016/j.bbadis.2015.06.008.
604 Mah, J.K., Korngut, L., Dykeman, J., Day, L., Pringsheim, T., and Jette, N. (2014). A systematic
605 review and meta-analysis on the epidemiology of Duchenne and Becker muscular dystrophy.
606 Neuromuscul Disord *24*, 482-491. 10.1016/j.nmd.2014.03.008.
607 Mareedu, S., Pachon, R., Thilagavathi, J., Fefelova, N., Balakrishnan, R., Niranjan, N., Xie, L.H., and
608 Babu, G.J. (2021). Sarcolipin haploinsufficiency prevents dystrophic cardiomyopathy in mdx mice.
609 Am J Physiol Heart Circ Physiol *320*, H200-h210. 10.1152/ajpheart.00601.2020.
610 Mavrogeni, S., Markousis-Mavrogenis, G., Papavasiliou, A., and Kolovou, G. (2015). Cardiac
611 involvement in Duchenne and Becker muscular dystrophy. World J Cardiol *7*, 410-414.
612 10.4330/wjc.v7.i7.410.
613 Mázala, D.A., Novak, J.S., Hogarth, M.W., Nearing, M., Adusumalli, P., Tully, C.B., Habib, N.F.,
614 Gordish-Dressman, H., Chen, Y.W., Jaiswal, J.K., and Partridge, T.A. (2020). TGF-β-driven muscle
615 degeneration and failed regeneration underlie disease onset in a DMD mouse model. JCI Insight
616 *5*. 10.1172/jci.insight.135703.
617 Mendell, J.R., Shilling, C., Leslie, N.D., Flanigan, K.M., al-Dahhak, R., Gastier-Foster, J., Kneile, K.,
618 Dunn, D.M., Duval, B., Aoyagi, A., et al. (2012). Evidence-based path to newborn screening for
619 Duchenne muscular dystrophy. Ann Neurol *71*, 304-313. 10.1002/ana.23528.
620 Robert, V., Massimino, M.L., Tosello, V., Marsault, R., Cantini, M., Sorrentino, V., and Pozzan, T.
621 (2001). Alteration in calcium handling at the subcellular level in mdx myotubes. J Biol Chem *276*,
622 4647-4651. 10.1074/jbc.M006337200.
623 Santulli, G., Lewis, D., des Georges, A., Marks, A.R., and Frank, J. (2018). Ryanodine Receptor
624 Structure and Function in Health and Disease. Subcell Biochem *87*, 329-352. 10.1007/978-981-
625 10-7757-9_11.
626 Schneider, J.S., Shanmugam, M., Gonzalez, J.P., Lopez, H., Gordan, R., Fraidenraich, D., and Babu,
627 G.J. (2013). Increased sarcolipin expression and decreased sarco(endo)plasmic reticulum Ca2+

628 uptake in skeletal muscles of mouse models of Duchenne muscular dystrophy. J Muscle Res Cell
629 Motil *34*, 349-356. 10.1007/s10974-013-9350-0.
630 Shin, J., Tajrishi, M.M., Ogura, Y., and Kumar, A. (2013). Wasting mechanisms in muscular
631 dystrophy. Int J Biochem Cell Biol *45*, 2266-2279. 10.1016/j.biocel.2013.05.001.
632 Smith, W.S., Broadbridge, R., East, J.M., and Lee, A.G. (2002). Sarcolipin uncouples hydrolysis of
633 ATP from accumulation of Ca2+ by the Ca2+-ATPase of skeletal-muscle sarcoplasmic reticulum.
634 Biochem J *361*, 277-286.
635 Strakova, J., Kamdar, F., Kulhanek, D., Razzoli, M., Garry, D.J., Ervasti, J.M., Bartolomucci, A., and
636 Townsend, D. (2018). Integrative effects of dystrophin loss on metabolic function of the mdx
637 mouse. Scientific Reports *8*, 13624. 10.1038/s41598-018-31753-3.
638 Straub, V., Balabanov, P., Bushby, K., Ensini, M., Goemans, N., De Luca, A., Pereda, A., Hemmings,
639 R., Campion, G., Kaye, E., et al. (2016). Stakeholder cooperation to overcome challenges in
640 orphan medicine development: the example of Duchenne muscular dystrophy. Lancet Neurol *15*,
641 882-890. 10.1016/s1474-4422(16)30035-7.
642 Swiderski, K., and Lynch, G.S. (2021). Murine models of Duchenne muscular dystrophy: is there a
643 best model? Am J Physiol Cell Physiol *321*, C409-c412. 10.1152/ajpcell.00212.2021.
644 Tubridy, N., Fontaine, B., and Eymard, B. (2001). Congenital myopathies and congenital muscular
645 dystrophies. Curr Opin Neurol *14*, 575-582. 10.1097/00019052-200110000-00005.
646 Tupling, A.R. (2004). The sarcoplasmic reticulum in muscle fatigue and disease: role of the
647 sarco(endo)plasmic reticulum Ca2+-ATPase. Can J Appl Physiol *29*, 308-329.
648 Tupling, A.R. (2009). Excitation-Contraction Coupling. In Encyclopedia of Neuroscience, M.
649 Binder, N. Hirokawa, and U. Windhorst, eds. (Springer Berlin Heidelberg), pp. 1479-1483.
650 10.1007/978-3-540-29678-2_3191.
651 Turner, P.R., Westwood, T., Regen, C.M., and Steinhardt, R.A. (1988). Increased protein
652 degradation results from elevated free calcium levels found in muscle from mdx mice. Nature
653 *335*, 735-738. 10.1038/335735a0.
654 van Putten, M., Putker, K., Overzier, M., Adamzek, W.A., Pasteuning-Vuhman, S., Plomp, J.J., and
655 Aartsma-Rus, A. (2019). Natural disease history of the D2-mdx mouse model for Duchenne
656 muscular dystrophy. FASEB J *33*, 8110-8124. 10.1096/fj.201802488R.
657 Viner, R.I., Ferrington, D.A., Huhmer, A.F., Bigelow, D.J., and Schoneich, C. (1996). Accumulation
658 of nitrotyrosine on the SERCA2a isoform of SR Ca-ATPase of rat skeletal muscle during aging: a
659 peroxynitrite-mediated process? FEBS Lett *379*, 286-290.
660 Viner, R.I., Ferrington, D.A., Williams, T.D., Bigelow, D.J., and Schoneich, C. (1999a). Protein
661 modification during biological aging: selective tyrosine nitration of the SERCA2a isoform of the
662 sarcoplasmic reticulum Ca2+-ATPase in skeletal muscle. Biochem J *340 (Pt 3)*, 657-669.
663 Viner, R.I., Krainev, A.G., Williams, T.D., Schoneich, C., and Bigelow, D.J. (1997). Identification of
664 oxidation-sensitive peptides within the cytoplasmic domain of the sarcoplasmic reticulum Ca2+-
665 ATPase. Biochemistry *36*, 7706-7716. 10.1021/bi970058z
666 bi970058z [pii].
667 Viner, R.I., Williams, T.D., and Schoneich, C. (1999b). Peroxynitrite modification of protein thiols:
668 oxidation, nitrosylation, and S-glutathiolation of functionally important cysteine residue(s) in the
669 sarcoplasmic reticulum Ca-ATPase. Biochemistry *38*, 12408-12415. bi9909445 [pii].
670 Voit, A., Patel, V., Pachon, R., Shah, V., Bakhutma, M., Kohlbrenner, E., McArdle, J.J., Dell'Italia,
671 L.J., Mendell, J.R., Xie, L.H., et al. (2017). Reducing sarcolipin expression mitigates Duchenne

672 muscular dystrophy and associated cardiomyopathy in mice. Nat Commun *8*, 1068.
673 10.1038/s41467-017-01146-7.
674 Yeh, Y.H., Kuo, C.T., Chan, T.H., Chang, G.J., Qi, X.Y., Tsai, F., Nattel, S., and Chen, W.J. (2011).
675 Transforming growth factor-β and oxidative stress mediate tachycardia-induced cellular
676 remodelling in cultured atrial-derived myocytes. Cardiovasc Res *91*, 62-70. 10.1093/cvr/cvr041.
677
678
679

Figure 1

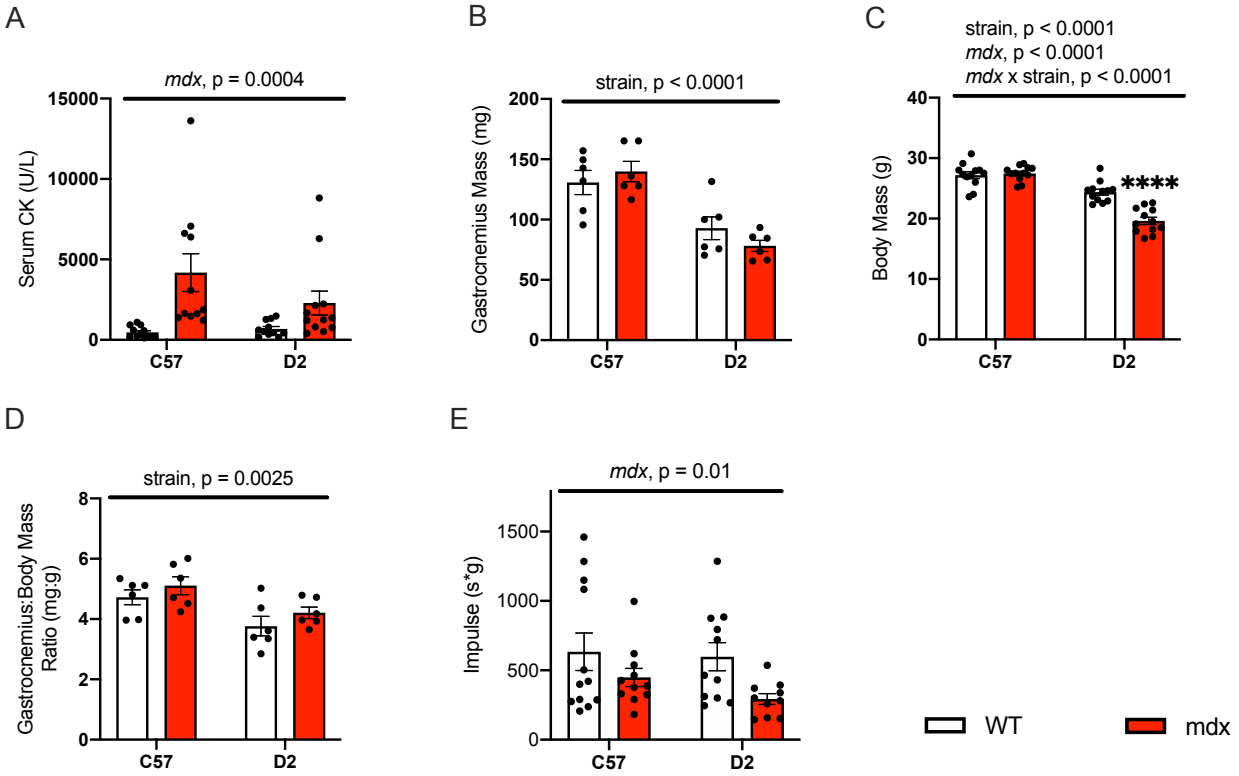
A
mdx, p = 0.0004
Serum CK (U/L)
15000
10000
5000
0
C57
D2
B
strain, p < 0.0001
Gastrocnemius Mass (mg)
200
150
100
50
0
C57
D2
C
strain, p < 0.0001
mdx, p < 0.0001
mdx x strain, p < 0.0001
Body Mass (g)
40
30
20
10
0
****
C57
D2
D
strain, p = 0.0025
Gastrocnemius:Body Mass Ratio (mg:g)
8
6
4
2
0
C57
D2
E
mdx, p = 0.01
Impulse (s*g)
1500
1000
500
0
C57
D2
WT
mdx

Figure 2

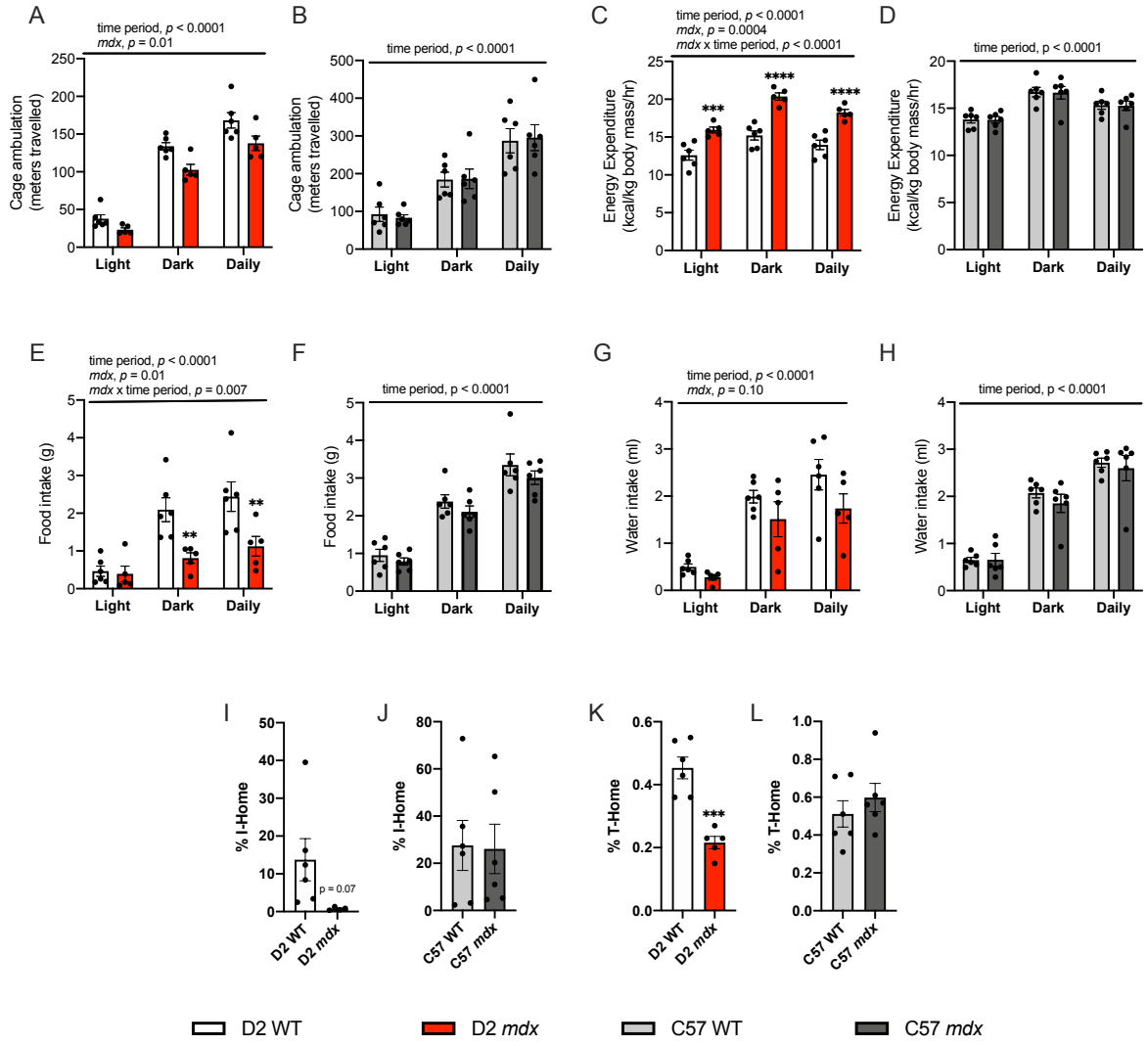
A
time period, p < 0.0001
mdx, p = 0.01
Cage ambulation (meters travelled)
Light
Dark
Daily
B
time period, p < 0.0001
Cage ambulation (meters travelled)
C
time period, p < 0.0001
mdx, p = 0.0004
mdx x time period, p < 0.0001
Energy Expenditure (kcal/kg body mass/hr)
D
time period, p < 0.0001
Energy Expenditure (kcal/kg body mass/hr)
E
time period, p < 0.0001
mdx, p = 0.01
mdx x time period, p = 0.007
Food intake (g)
F
time period, p < 0.0001
Food intake (g)
G
time period, p < 0.0001
mdx, p = 0.10
Water intake (ml)
H
time period, p < 0.0001
Water intake (ml)
I
% I-Home
p = 0.07
D2 WT
D2 mdx
J
% I-Home
C57 WT
C57 mdx
K
% T-Home
D2 WT
D2 mdx
L
% T-Home
C57 WT
C57 mdx
D2 WT
D2 mdx
C57 WT
C57 mdx

686 Figure 3

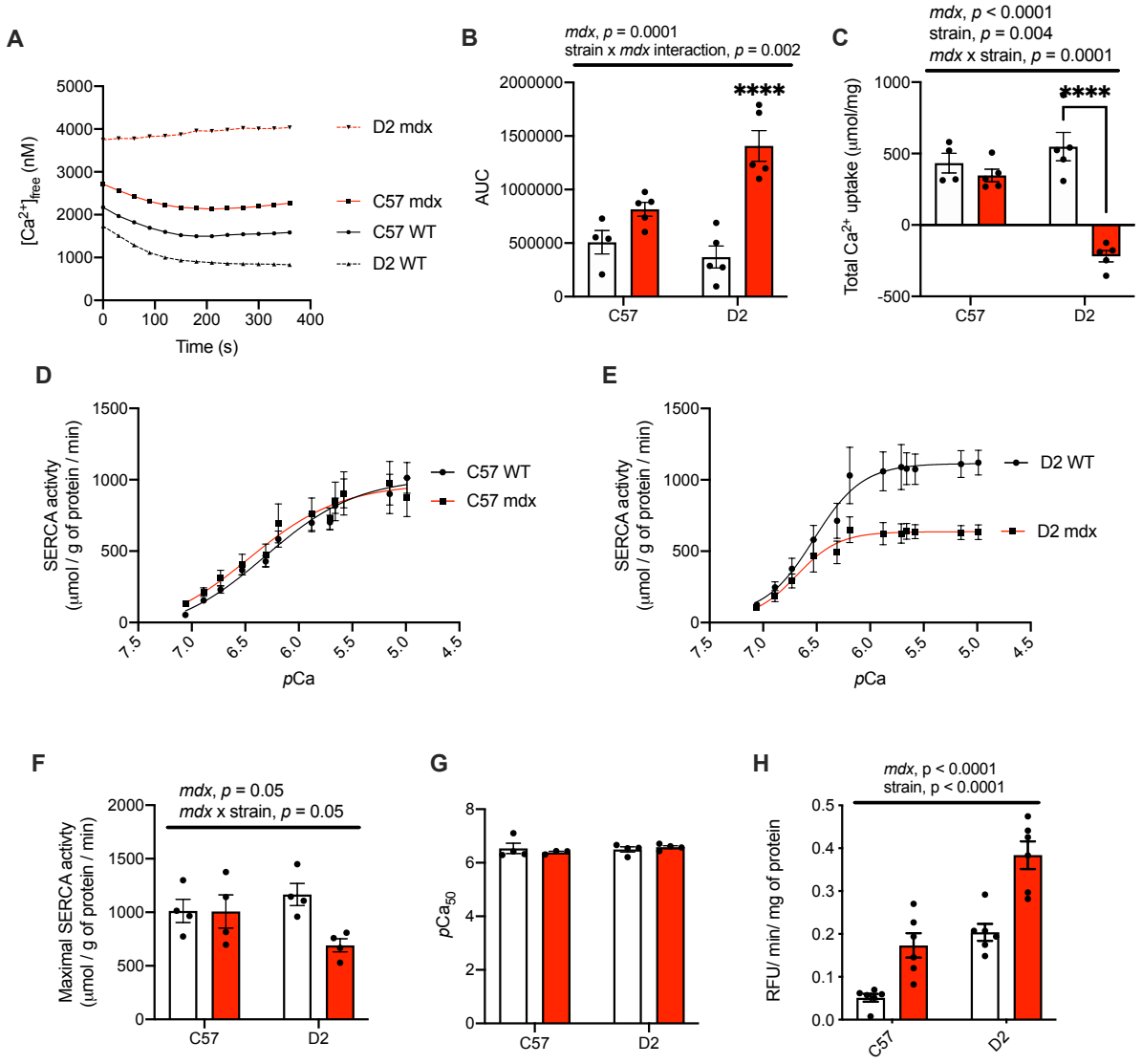

687
688
689

Figure 4

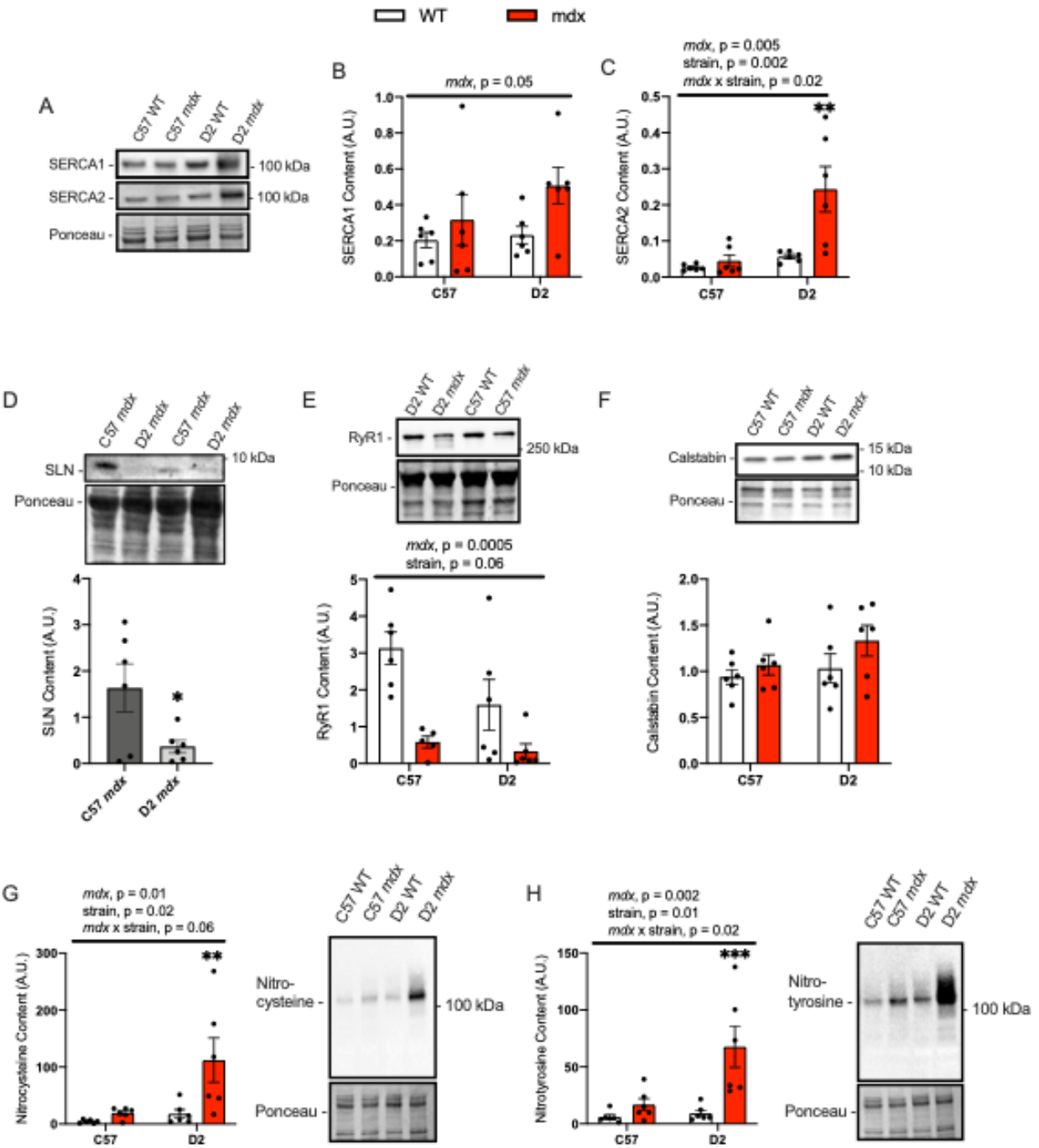
WT
mdx
A
C57 WT
C57 mdx
D2 WT
D2 mdx
SERCA1
SERCA2
Ponceau
100 kDa
100 kDa
B
mdx, p = 0.05
SERCA1 Content (A.U.)
C57
D2
C
mdx, p = 0.005
strain, p = 0.002
mdx x strain, p = 0.02
SERCA2 Content (A.U.)
D
SLN
10 kDa
SLN Content (A.U.)
E
RyR1
250 kDa
mdx, p = 0.0005
strain, p = 0.06
RyR1 Content (A.U.)
F
Calstabin
15 kDa
10 kDa
Calstabin Content (A.U.)
G
mdx, p = 0.01
strain, p = 0.02
mdx x strain, p = 0.06
Nitrocysteine Content (A.U.)
Nitro-cysteine
H
mdx, p = 0.002
strain, p = 0.01
mdx x strain, p = 0.02
Nitrotyrosine Content (A.U.)
Nitro-tyrosine

Figure 5

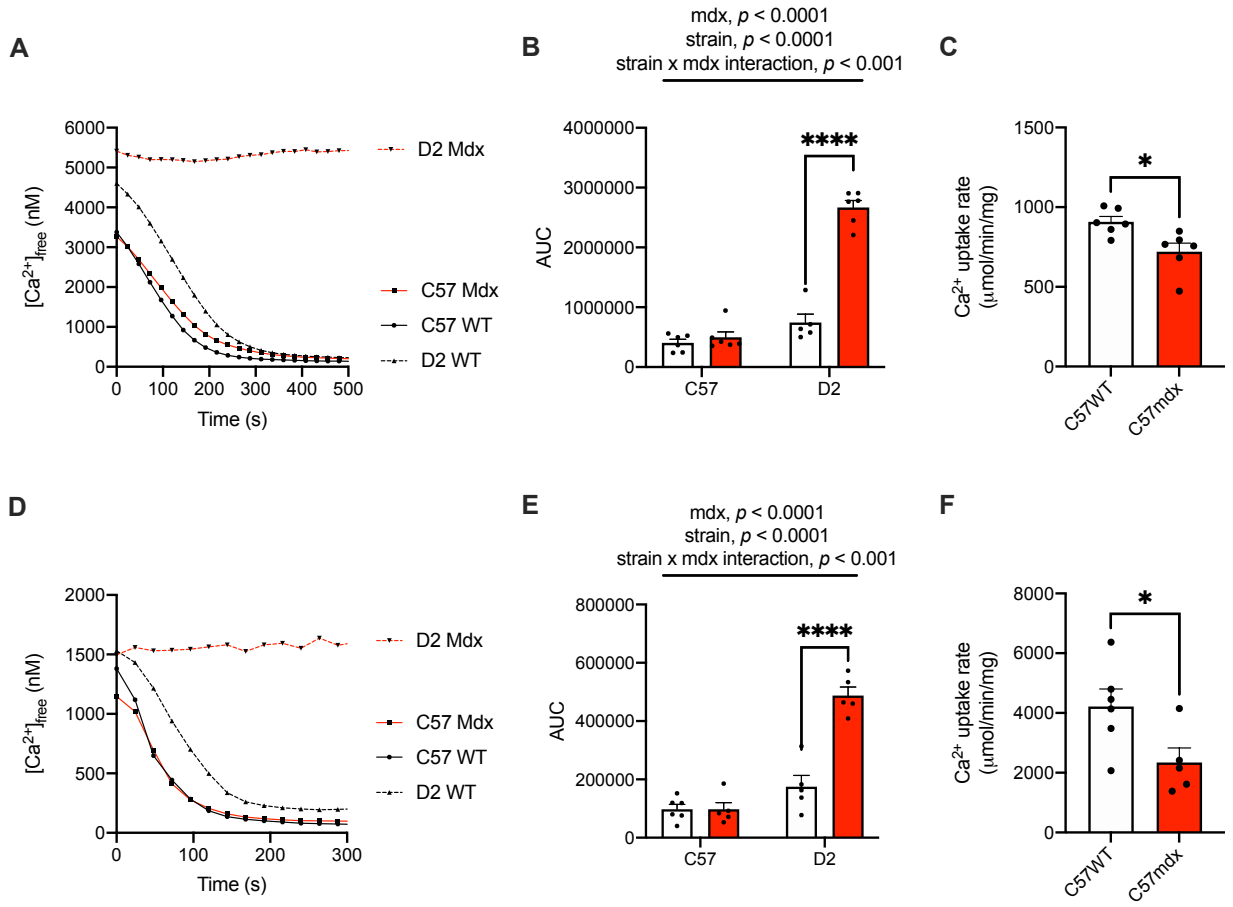
A
B
C
D
E
F
mdx, p < 0.0001
strain, p < 0.0001
strain x mdx interaction, p < 0.001
[Ca2+]free (nM)
Time (s)
D2 Mdx
C57 Mdx
C57 WT
D2 WT
AUC
C57
D2
****
Ca2+ uptake rate (µmol/min/mg)
C57WT
C57mdx
*